NUCL SCI TECH (2018) 29:55
https://doi.org/10.1007/s41365-018-0394-0

Model-based cross section calculations on production of ^{43,34}Sc, ^{45}Ti, ^{51}Cr, ^{54}Mn, and ^{55}Fe radioisotopes

Mustafa Yiğit[1]

Received: 23 September 2017 / Revised: 14 December 2017 / Accepted: 26 December 2017 / Published online: 16 March 2018

Abstract A cross section database on excitation functions of reactions produced by charged particles is essential for many areas of nuclear research. Particularly, accurate knowledge on nuclear cross sections for the cyclotron production of radioisotopes is very important for nuclear medicine. In the present paper, the cross section calculations for the production of ^{43,44}Sc, ^{45}Ti, ^{51}Cr, ^{54}Mn, and ^{55}Fe radioisotopes were carried out by the use of ALICE/ASH code using the Fermi gas model, Kataria Ramamurthy Fermi gas model, and superfluid nuclear model for nuclear level density. Thereby, these model calculations were compared with the available measured data.

Keywords Radioisotope production · Scandium-44 · Chromium-51 · Superfluid nuclear model · Cross section

1 Introduction

Nuclear data are needed to explain the nature of the internal structure of nuclei. Nuclear physics researches are focused on understanding nuclear data, which are crucial for many applications such as fusion, fission, radiation therapy, accelerator-driven system (ADS), radiobiology, nuclear wear measurement, astrophysics, and cosmochemistry [1–10]. Data relevant to radioisotopes can be grouped under two headings, the nuclear reaction data and decay data. Since the decay data have been well established, the nuclear reaction data need to be further studied [2, 5, 11]. The nuclear reaction cross section data include a wide range of projectile energies from a few MeV up to the region of several GeV [2]. Obviously, the nuclear reaction data are indispensable items for radionuclide production. On the other hand, because cyclotrons generate very little radioactive waste, they are powerful sources with minimal environmental impact. Furthermore, the cyclotrons are very important in providing radioisotopes by different reaction mechanisms based on bombarding the target nuclei with charged particles for nuclear medicine [12]. The radioisotopes ^{43,44}Sc, ^{45}Ti, ^{51}Cr, ^{54}Mn, and ^{55}Fe nuclei have been used in the various fields. The positron-emitting radioisotope ^{43}Sc (with a half-life of 3.89 h) could be used for an in vivo dosimetry [13]. The half-life (3.97 h) of ^{44}Sc and its high positron branching of 94.27% may stimulate the practice of ^{44}Sc-labelled PET radiopharmaceuticals [14]. Because the ^{44}Sc has longer half-life than ^{68}Ga (67.71 min), it can be a useful alternative to ^{68}Ga as a positron emitter [12, 15], and also it is the most interesting nuclear radioisotope for medical imaging using $\beta^+\gamma$ coincidences [13]. The radioisotope ^{54}Mn has a half-life of 312.3 days and decays by electron capture. It emits a single gamma ray at an energy of 834.8 keV. The ^{54}Mn is generally used as a standard source for γ-ray detectors [16]. The radioisotope ^{55}Fe ($T_{1/2}$=2.73 years) decays by electron capture, and the major radiation emitted is the K_α X-ray with an energy of 5.89 keV. The ^{55}Fe is generally used as a standard source for X-ray detectors. The ^{51}Cr radioisotope with a half-life of 27.7 days decays by electron capture. The decay results in the emission of a gamma ray of energy 320 keV. The ^{51}Cr has been used to label red blood cells for the measurement of mass or volume of a living system and tracer investigations [16]. The radioisotope ^{45}Ti with a

✉ Mustafa Yiğit
mustafayigit@aksaray.edu.tr

[1] Department of Physics, Aksaray University, 68100 Aksaray, Turkey

half-life of 3.08 h decays 85% by positron emission and 15% by electron capture. The positron decay of the radioisotope ^{45}Ti proceeds mainly to the ground state of ^{45}Sc, so that almost no other concurrent γ-rays are emitted apart from the two annihilation photons. Thus, this radioisotope is suitable for PET [17]. In the present study, the excitation curves for the production of ^{43,44}Sc, ^{45}Ti, ^{51}Cr, ^{54}Mn, and ^{55}Fe radioisotopes via nuclear reactions induced by proton particles were calculated using the ALICE/ASH nuclear reaction code [18] and compared with the measured values [19] and TENDL-2015 data [20]. In this context, there exist similar studies with different particle-induced reactions in the literature [21–25]. In this paper, especially, the effects on the calculated cross section data of the variation in nuclear level densities have been investigated for the production of the considered radioisotopes.

2 Computational method

The ALICE/ASH nuclear reaction code developed by Broeders et al. [18] is a modified version of the code ALICE/91. The ALICE/ASH is a reaction code describing the fast γ-emissions, the pre-compound composite particle emissions, the fission fragment yield calculations, and the nuclear level density calculations. Furthermore, this code is useful for cross section predictions using compound and pre-compound reaction mechanisms, angular and energy distributions of secondary particles at reactions induced by nuclei and nucleons with the incoming energy up to 300 MeV [18]. It is known that the reaction mechanism depends on the energies of incident particles [26–32]. Compound nuclear effects for a given reaction dominate in the incident energy range of about 0–10 MeV. The compound emission was described with the Weisskopf–Ewing model [33] without angular momentum conservation. The basic physical parameters in this model are inverse reaction cross section, level density parameter, nuclear binding energy, and pairing. In the Weisskopf–Ewing approximation, the evaporation cross sections for initial channel "a" and final channel "b" are given by

$$\sigma_{ab}^{\mathrm{WE}} = \sigma_{ab}(E_{\mathrm{inc}})\Gamma_b \Big/ \sum_{b'} \Gamma_{b'}, \tag{1}$$

where the term "E_{inc}" is incident particle energy, and the term "Γ_b" represents emission probability per unit time of a particle of type "b" by the compound nucleus. The emission probability is calculated by the formula $\Gamma_b = \frac{2s_b+1}{\pi^2\hbar^2}\mu_b \int d\varepsilon \sigma_b^{\mathrm{inv}}(\varepsilon)\varepsilon\frac{\omega_1(U)}{\omega_1(E)}$. The term "$U$" denotes excitation energy of residual nucleus, the term "s_b" is spin, the term "μ_b" is reduced mass, the term "σ_b^{inv}" is inverse reaction cross section, and the term "ω_1" is total nuclear level density [33].

The pre-equilibrium nuclear effects dominate in the reactions produced by light particles with a projectile energy range above about 8–10 MeV. This process takes place in a number of steps, corresponding to the excitation of successive particle–hole pairs via the interaction of the target nucleus and projectile. For the pre-equilibrium nuclear reaction process, the Blann's Hybrid model was written in the following form [34],

$$\frac{d\sigma_\upsilon(\varepsilon)}{d\varepsilon} = \sigma_{\mathrm{R}} P_\upsilon(\varepsilon), \tag{2}$$

$$P_\upsilon(\varepsilon)d\varepsilon = \sum_{\substack{n=n_0 \\ \Delta n=+2}}^{\bar{n}} \left[{}_n\chi_\upsilon N_n(\varepsilon, U)/N_n(E)\right] g_v\, d\varepsilon \left[\lambda_c(\varepsilon)/(\lambda_c(\varepsilon) + \lambda_+(\varepsilon))\right] D_n, \tag{3}$$

where the term "σ_{R}" denotes the nuclear reaction cross section, the term "${}_n\chi_v$" is the particle number of the "v" type (neutron or proton) with "n" exciton hierarchy, the term "g_v" represents the single-particle level density for "v" type, and the term "$P_\upsilon(\varepsilon)d\varepsilon$" corresponds to the particle number of the "v" type emitted into the unbound continuum with the energy between "ε" and "$\varepsilon + d\varepsilon$". The first set of square brackets of Eq. (3) represents the particle number to be found at a given energy "ε" for all scattering situations leading to an "n" exciton configuration. Moreover, the second set of square brackets in this equation corresponds to the fraction of particles with the "v" type at an energy which should undergo emission into the continuum, rather than making an intranuclear transition. The terms "$\lambda_+(\varepsilon)$" and "$\lambda_c(\varepsilon)$" represent the intranuclear transition and emission rates, respectively. The terms "U" and "E" represent the excitation energies of the residual nucleus and composite system, respectively. Physically, the term "D_n" is the average fraction of the initial population surviving to the exciton number being treated [34]. Moreover, the geometry-dependent hybrid (GDH) model is a nuclear reaction model that takes into account nuclear geometry properties like the diffuseness of the nuclear surface. So, this model takes into consideration the reduced matter density and the shallow potential at the nuclear surface. The differential emission spectra in this model were described in the following form,

$$\frac{d\sigma_v(\varepsilon)}{d\varepsilon} = \pi \lambda\!\!\!^{-2} \sum_{\ell=0}^{\infty}(2\ell+1)T_\ell P_v(\ell,\varepsilon), \tag{4}$$

where the term "T_ℓ" denotes the transmission coefficient for the ℓth partial wave, and the term "$\lambda\!\!\!^{-}$" denotes the reduced de Broglie wavelength of the incident particle.

This model is made according to incoming orbital angular momentum "ℓ" in order to account for the nuclear effects of density distribution [34, 35].

The combinatorics of a Fermi gas plus pairing has been widely suggested for calculating the nuclear level densities. The level density of the Fermi gas model (FGM) with an energy-dependent nuclear level density parameter proposed by Ignatyuk et al. [36] is given in the following form,

$$\rho(U) \propto a^{-1/4}(U-\delta)^{-5/4}e^{\left(2\sqrt{a(U-\delta)}\right)}. \quad (5)$$

Here, the level density parameter "a" is given by the phenomenological expression [36]

$$a(U) = \tilde{a}\left(1 + \frac{f(U)\delta W}{U}\right), \quad (6)$$

where the term $\tilde{a}$ corresponds to the asymptotic value of the nuclear level density parameter. The term "δW" represents shell correction [18]. The nuclear level density in the superfluid nuclear model (SFM) [37] is presented by the expression

$$\rho(U) = \rho_{qp}(U')K_{vib}(U')K_{rot}(U'), \quad (7)$$

where the terms $K_{rot}(U')$ and $K_{vib}(U')$ represent rotational and vibrational enhancement factors at effective nuclear excitation energy "U'", respectively. The term $\rho_{qp}(U')$ is the density of quasi-particle excitation [18]. The shell structure of the nucleus in the Kataria Ramamurthy Fermi gas model (KRM) [38] has quite important effects on level densities of the excited nucleus. The KRM is defined by the semi-empirical formula in terms of a Fourier expansion of single-particle level densities of nucleons in the nuclei. The nuclear level density parameter "a" in this model is given by the expression

$$a = \alpha A\left(1 - \beta A^{-\frac{1}{3}}\right). \quad (8)$$

The level density parameter is dependent upon the well parameters and also has been given by separation energies in the following form,

$$a = \alpha A + A^{\frac{2}{3}}\left[\beta_0 + \frac{\beta_1}{S_n} + \frac{\beta_2}{S_p}\right], \quad (9)$$

where the terms "s_p" and "s_n" denote the proton and neutron separation energies, respectively. The "β_0", "β_1", "β_2", and "α" are the fitting parameters [38].

3 Results and discussion

The calculated cross section values of the ^{45}Sc(p, n) ^{45}Ti, ^{45}Sc(p, np) ^{44}Sc, ^{45}Sc(p, 2np) ^{43}Sc, ^{55}Mn(p, np) ^{54}Mn, ^{55}Mn (p, n) ^{55}Fe, and ^{55}Mn(p, nα) ^{51}Cr nuclear reaction processes in comparison with the existing experimental values are graphically given in Figs. 1, 2, 3, 4, 5, and 6. In these calculations, the various level density models such as the FGM, SFM, and KRM in the ALICE/ASH nuclear reaction code were used. Additionally, the effects of the level density parameter on the calculated excitations functions are investigated via four level density parameters such as $a = A/6$, $A/12$, $A/18$, and $A/24$ values in the FGM.

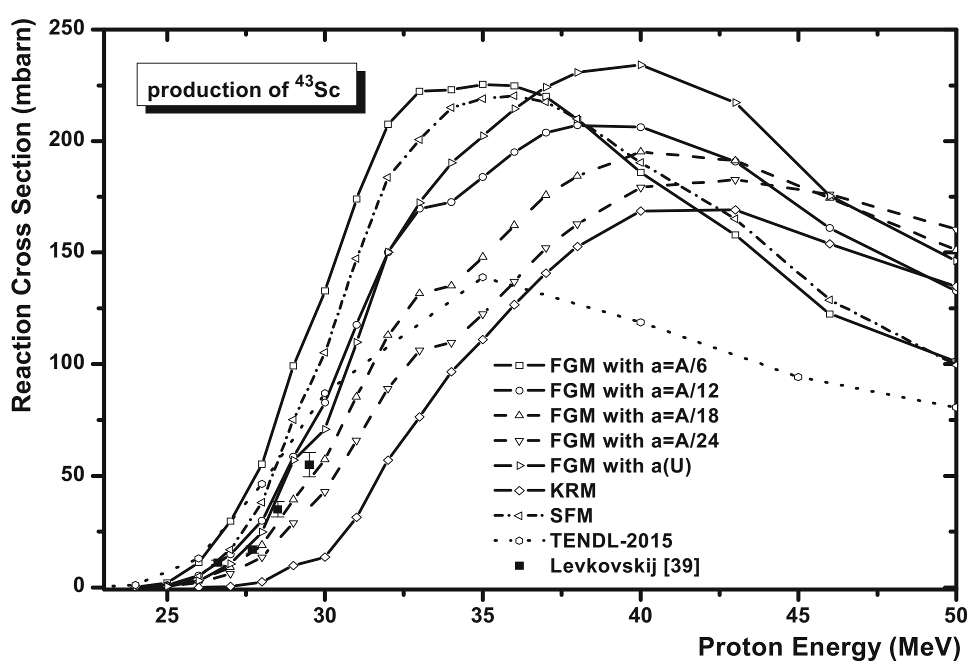

Fig. 1 Nuclear model calculation results for the ^{45}Sc(p, 2np) ^{43}Sc reaction compared with the measured excitation functions

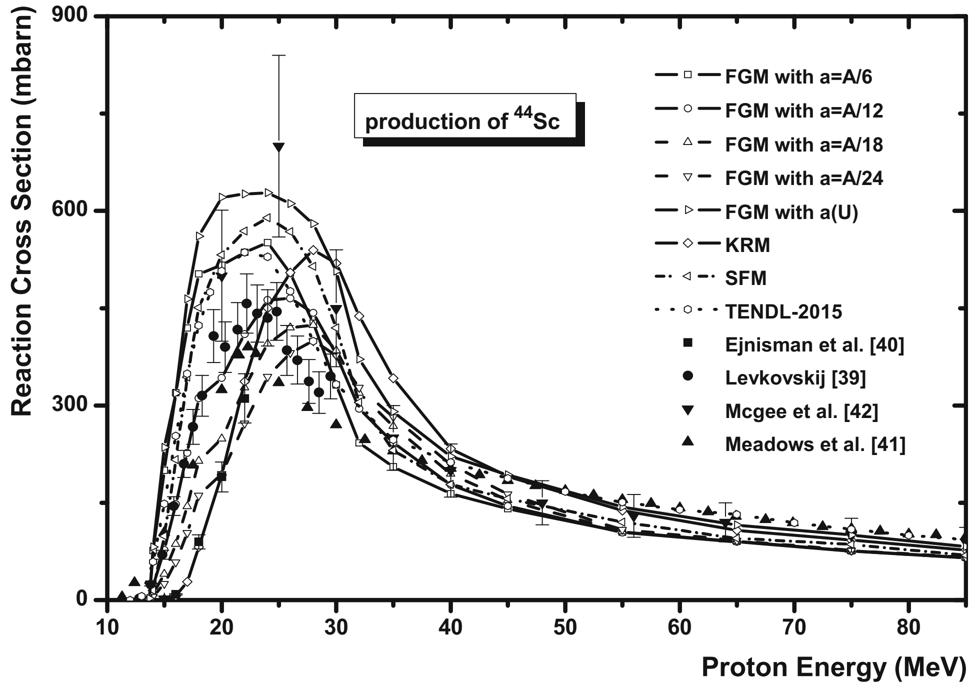

Fig. 2 Nuclear model calculation results for the ^{45}Sc(p, np) ^{44}Sc reaction compared with the measured excitation functions

3.1 Production of ^{43}Sc radioisotope

The nuclear cross section values of the ^{45}Sc (p, 2np) ^{43}Sc reaction, up to an incident energy of 50 MeV, are presented in Fig. 1. Four experimental values for the investigated reaction are presented by Levkovskij [39] in the incident energy range of 26.6–29.5 MeV. One can see from Fig. 1 that the shape and values of excitation functions are highly sensitive to the choice of the level density formulae and parameters. Here, cross section data of 11 ± 1.1 mb at an incident energy of 26.6 MeV reported by Levkovskij [39] are in very good agreement with the cross section values estimated by the SFM and FGM (with $a = A/12$) models based on level density. Besides, the agreement between the other three cross section data of Levkovskij [39] and the FGM calculations with level density parameter $a = A/18$ is quite good, generally within the error bars. Moreover, because the excitation function estimated by the KRM has very low cross sections, it is not in agreement with the measured data obtained by Levkovskij [39].

3.2 Production of the ^{44}Sc radioisotope

The nuclear excitation curves for the ^{45}Sc (p, np) ^{44}Sc reaction are shown in Fig. 2 up to a proton energy of 85 MeV. Four data obtained by Ejnisman et al. [40] in the incident energy range of 16–22 MeV are in very good agreement with the predictions obtained using the KRM level density. Moreover, the cross section results of the level density parameter with $a = A/12$ using the FGM in the energy range of 12.8–24.8 MeV are in general agreement with the data obtained by Levkovskij [39] and are within the error bars. The cross section estimations obtained using the SFM and FGM (with $a(U)$) level densities using the code ALICE/ASH are mostly in good agreement with the measured cross sections of Mcgee et al. [42] in the proton energy region of 15–85 MeV. However, the excitation functions predicted using the code ALICE/ASH are not very consistent with the shape of the measured excitation function of Meadows et al. [41] for the considered reaction. The calculated excitation functions have maximum cross sections in the incident energy range 20–30 MeV. Also, in the peak portion of the excitation functions, we can observe important discrepancies between the calculations of different level density models.

3.3 Production of ^{45}Ti radioisotope

The cross sections calculated in the present paper and experimental values obtained by Levkovskij [39], Thomas and Bartolini [44], Howard et al. [43], Ejnisman et al. [40], and Mcgee et al. [42] are plotted in Fig. 3 for the ^{45}Sc (p, n) ^{45}Ti reaction. The cross section results predicted by the FGM with $a(U)$ show a good overall agreement with two experimental values of Ejnisman et al. [40] at the energies of 16–20 MeV. However, at the energies of 18–22 MeV, the data measured by Ejnisman et al. [40] are in good agreement with the cross section results calculated using the FGM with $a = A/24$ for the investigated reaction. The

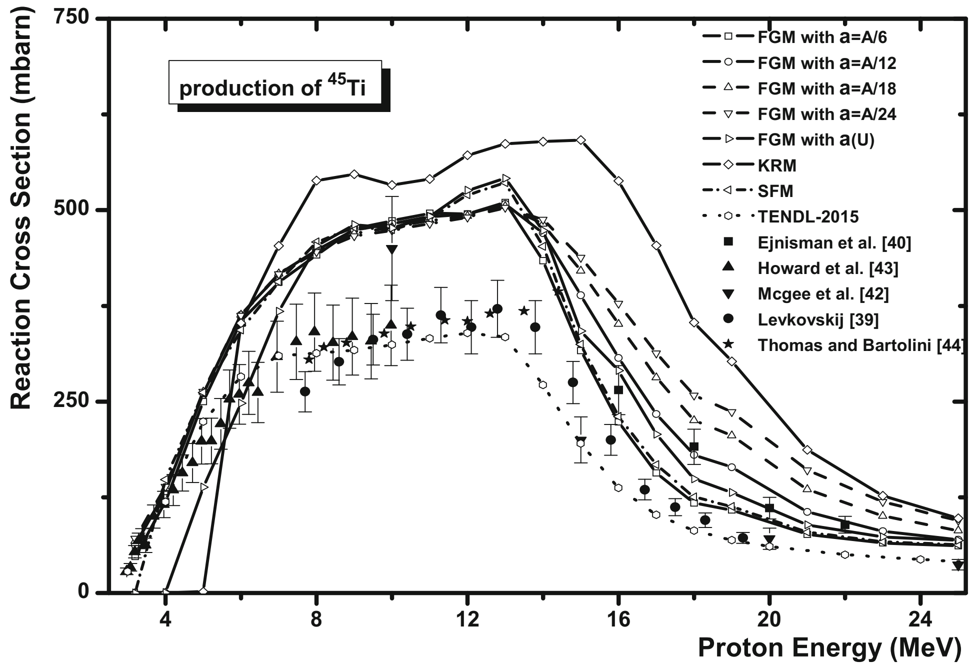

Fig. 3 Nuclear model calculation results for the ^{45}Sc(p, n) ^{45}Ti reaction compared with the measured excitation functions

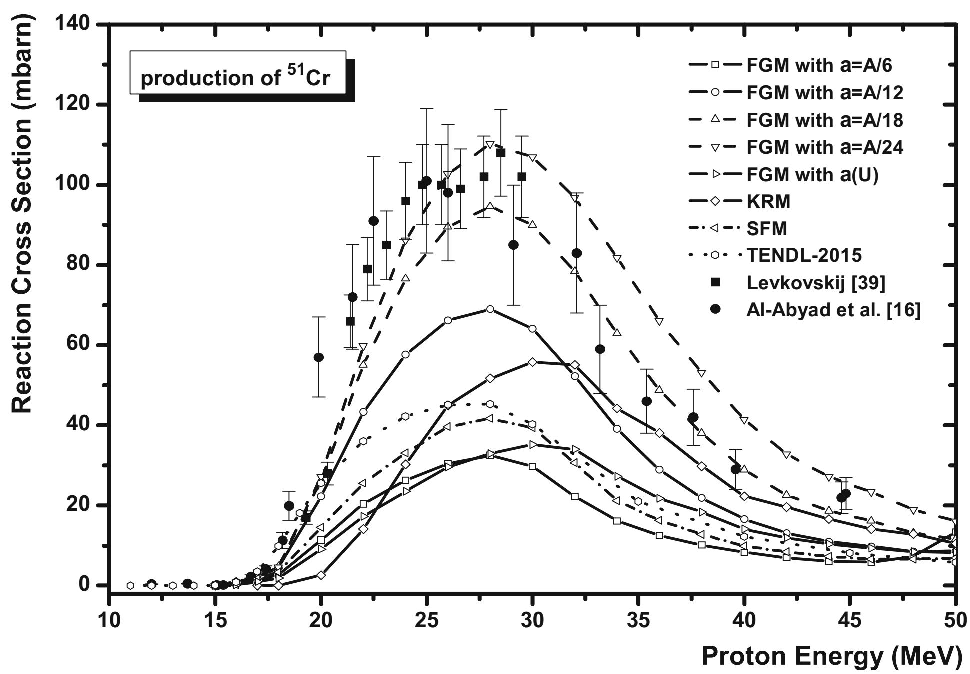

Fig. 4 Nuclear model calculation results for the ^{55}Mn(p, nα) ^{51}Cr reaction compared with the measured excitation functions

excitation curves for the ^{45}Sc (p, n) ^{45}Ti reaction reach maximum values in the proton energy region of 8–15 MeV and decrease above this incident energy region. Generally, the shape of the predicted cross sections at the maximum region of excitation functions is in agreement with each other. The excitation function estimated by the KRM level density shows a maximum of 591.5 mb at 15 MeV. The cross section of 450 ± 68 mb at an incident energy of 10 MeV obtained by Mcgee et al. [42] is in general agreement with the predictions of the FGM and SFM level densities. However, the cross sections of Mcgee et al. [42] at proton energies of 15, 20, and 25 MeV are quite a bit lower than the excitation functions estimated using the code ALICE/ASH. Besides, the data measured by Levkovskij [39] and Thomas and Bartolini [44], except for the value of 394 mb at a proton energy of 14.4 MeV, have lower results than the FGM, KRM, and SFM predictions by the code ALICE/ASH. At incident proton energies below

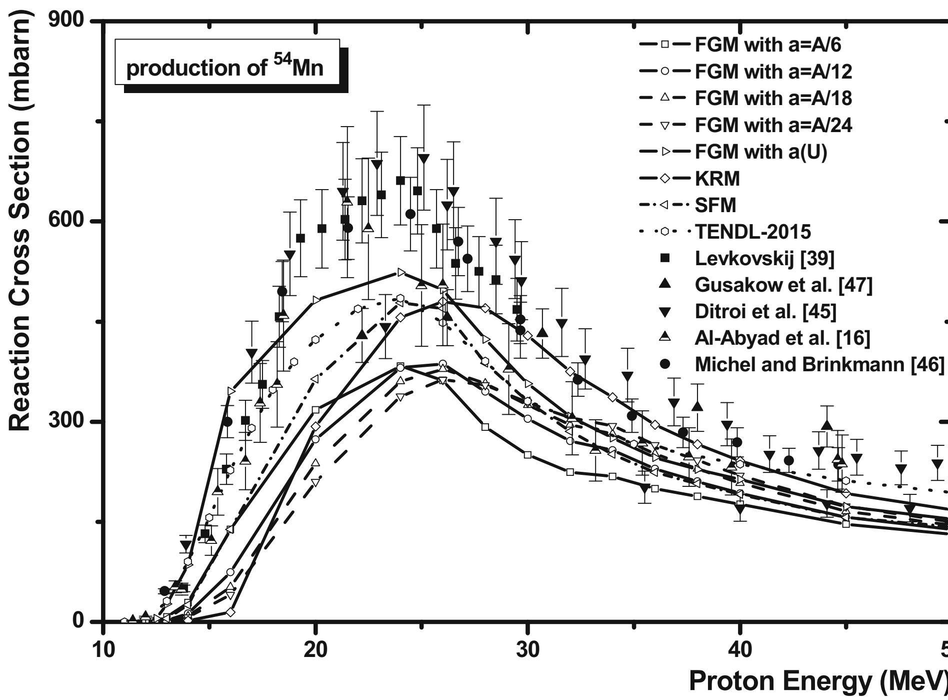

Fig. 5 Nuclear model calculation results for the $^{55}Mn(p,np)\ ^{54}Mn$ reaction compared with the measured excitation functions

7 MeV, the excitation function obtained by Howard et al. [43] yields an acceptable harmony with the theoretical cross section values within the error bars.

3.4 Production of ^{51}Cr radioisotope

In Fig. 4, the excitation function data for production of the ^{51}Cr radioisotope via the $^{55}Mn(p,n\alpha)\ ^{51}Cr$ reaction are plotted for comparison with the measured data in the literature up to the incident energy of 50 MeV. The cross section data obtained using level density parameters $a = A/18$ to $A/24$ in the FGM agree with the cross sections measured by Levkovskij [39] and Al-Abyad et al. [16] within the error bars. The excitation functions for the $^{55}Mn(p,n\alpha)\ ^{51}Cr$ nuclear reaction have maximum values in the proton energy range of 23–35 MeV. The calculated excitation functions via different level density parameters in the FGM using ALICE/ASH code differ greatly with each other at the maximum cross section region. For instance, at proton energy of 28 MeV, the cross section value calculated by the FGM level density with $a = A/24$ is 110.2 mb, whereas the cross section value predicted using the level density parameter $a = A/6$ is 32.5 mb.

3.5 Production of ^{54}Mn radioisotope

The comparison between the experimental and model results for cross sections of the $^{55}Mn(p,np)\ ^{54}Mn$ reaction is illustrated in Fig. 5. Excitation curves for this reaction have maximum position in the proton energy range of 20–30 MeV. The data calculated using the SFM, FGM, and KRM level densities via the code ALICE/ASH give lower results than the experimental data reported by Ditroi et al. [45], Levkovskij [39], and Michel and Brinkmann [46] at the maximum position of nuclear cross sections. However, these experimental data in the low energy ranges have an acceptable fit with theoretical cross section data predicted by the FGM with $a(U)$. In addition, the excitation function estimated using KRM level density by the ALICE/ASH code for this reaction gives good agreement within the statistical errors of the measured data of Ditroi et al. [45] and Michel and Brinkmann [46] in the proton energy range of 27–44 MeV except for the data of Ditroi et al. [45] at 35.5–40 MeV. However, the obtained cross sections using the level density parameter $a = A/6$ by the FGM at 35.5–40 MeV are in good agreement with two cross section data points measured by Ditroi et al. [45]. Furthermore, the FGM predictions with $a(U)$ have a good agreement with the experimental cross section values of Al-Abyad et al. [16] in the incident energy region of 11.4–44.8 MeV. The results of the KRM level density in the energy range of 22.2–38 MeV show closer agreement with the experimental values by Gusakow et al. [47] within the error bars.

3.6 Production of ^{55}Fe radioisotope

The comparison of the calculated and the experimental cross sections of the $^{55}Mn(p,n)\ ^{55}Fe$ reaction is presented in Fig. 6. Generally, the calculated excitation functions for this nuclear reaction have the similar spectral shape.

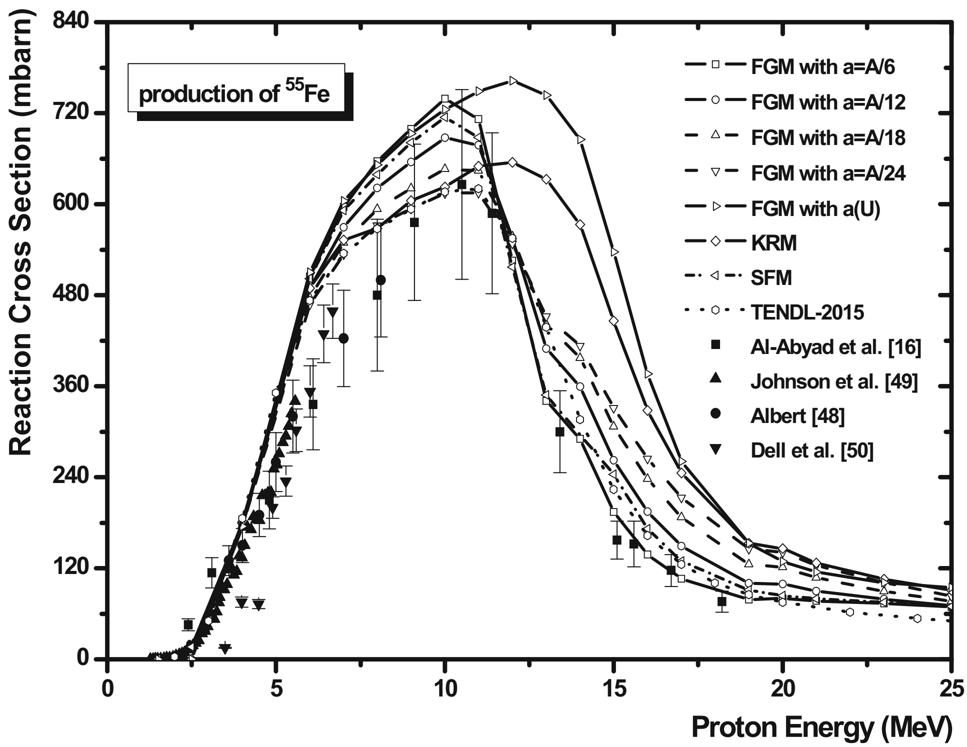

Fig. 6 Nuclear model calculation results for the ^{55}Mn(p, n) ^{55}Fe reaction compared with the measured excitation functions

However, the cross section values calculated by the FGM, KRM, and SFM level densities are different from each other at a peak portion of the nuclear excitation functions for the considered reaction. And also, the excitation functions for the ^{55}Mn (p, n) ^{55}Fe reaction have a maximum position in the proton energy range of 7–13 MeV. The excitation function estimated by the FGM level density with $a(U)$ shows a maximum of 762.6 mb at 12 MeV. The experimental measurements obtained by Albert [48] and Johnson et al. [49] are within the error bars and generally give an acceptable fit with theoretical model calculations. The excitation function of Dell et al. [50] in the proton energy range of 3.49–6.68 MeV for the considered nuclear reaction is quite a bit lower than the calculations of the ALICE/ASH code. However, a good agreement was established between the experimental cross section data of Al-Abyad et al. [16] and the excitation functions of the FGM (with $a = A/6$) and SFM level densities.

4 Conclusion

In this paper, the excitation functions for the nuclear reactions ^{45}Sc(p, n) ^{45}Ti, ^{45}Sc(p, np) ^{44}Sc, ^{45}Sc(p, 2np) ^{43}Sc, ^{55}Mn(p, np) ^{54}Mn, ^{55}Mn(p, n) ^{55}Fe, and ^{55}Mn(p, nα) ^{51}Cr have been investigated using the FGM, KRM, and SFM level densities by the code ALICE/ASH. The experimental values and the obtained model data are graphically given in Figs. 1, 2, 3, 4, 5, and 6. Generally, the cross sections predicted with the ALICE/ASH nuclear reaction code, except for the calculated cross sections for the ^{45}Sc(p, n) ^{45}Ti and ^{55}Mn(p, np) ^{54}Mn reactions at the maximum of excitation functions, are in fair agreement with the existing experimental results in the literature. We have observed that the cross sections can strongly vary with choice of the nuclear model parameters in the code. So, the size discrepancies between the calculated and the measured excitation functions can be reduced with the different level density models and level density parameters. Particularly, the shape of the excitation functions obtained with the SFM and FGM level densities, except for the maximum cross section region, follows the trend of the experimental cross sections. The obtained excitation functions contribute to the new investigations for radionuclide production.

References

1. F. Szelecsenyi, Measurement of cross sections of proton induced nuclear reactions on Ti, Ni, Zn, Cd, and Au up to 30 MeV and their application in radioisotope production, PhD Thesis (Lajos Kossuth University, Hungary) (1997)
2. S.M. Qaim, Radiochemical determination of nuclear data for theory and applications. J. Radioanal. Nucl. Chem. **284**, 489 (2010). https://doi.org/10.1007/s10967-010-0460-5
3. M. Yiğit, New empirical formulae for (n,t) cross sections at 14.6 MeV. Appl. Radiat. Isot. **128**, 307 (2017). https://doi.org/10.1016/j.apradiso.2017.07.047

4. M. Yiğit, Theoretical predictions of excitation functions of neutron-induced reactions on ^{6}Li, ^{9}Be, ^{12}C and ^{23}Na nuclei at low energies. J. Fusion Energy **34**, 140 (2015). https://doi.org/10.1007/s10894-014-9773-7
5. J. Luo, C. Wu, L. Jiang, L. He, Cross sections for d-^{3}H neutron interactions with samarium isotopes. Radiochim. Acta **104**, 523 (2016). https://doi.org/10.1515/ract-2016-0001
6. C. Yalçın, The cross section calculation of 112Sn(α, γ)116Te reaction with different nuclear models at the astrophysical energy range. Nucl. Sci. Tech. **28**, 113 (2017). https://doi.org/10.1007/s41365-017-0267-y
7. M. Yiğit, E. Tel, Theoretical determination of (d, n) and (d,2n) excitation functions of some structural fusion materials irradiated by deuterons. Nucl. Sci. Tech. **28**, 165 (2017). https://doi.org/10.1007/s41365-017-0316-6
8. C.W. Ma, J.L. Xu, An empirical formula for isotopic yield in Fe +p spallation reactions. J. Phys. G Nucl. Part Phys. **44**, 125101 (2017). https://doi.org/10.1088/1361-6471/aa90e6
9. C.W. Ma, C.J. Lv, G.Q. Zhang et al., Neutron-induced reactions on AlF_3 studied using the optical model. Nucl. Instrum. Methods Phys. Res. B **356–357**, 42 (2015). https://doi.org/10.1016/j.nimb.2015.04.060
10. C.J. Lv, C.W. Ma, Y.P. Liu, An investigation on γ induced activation reactions on human essential elements. Nucl. Sci. Tech. **26**, 030503 (2015). https://doi.org/10.13538/j.1001-8042/nst.26.030503
11. IAEA. Proceedings of the IAEA Consultants, Meeting on nuclear data for medical radioisotope production, Tokyo (Japan) (1987). http://www-nds.iaea.org/. Accessed 19 June 2017
12. M. Yiğit, E. Tel, Nuclear model calculation for production of ^{18}F, ^{22}Na, ^{44,46}Sc, ^{54}Mn, ^{64}Cu, ^{68}Ga, ^{76}Br and ^{90}Y radionuclides used in medical applications. Ann. Nucl. Energy **69**, 44 (2014). https://doi.org/10.1016/j.anucene.2014.01.036
13. M.U. Khandaker, K. Kim, M.W. Lee et al., Investigations of the natTi(p, x) 43,44 m,44 g,46,47,48Sc, 48 V nuclear processes up to 40 MeV. Appl. Rad. Isot. **67**, 1348 (2009). https://doi.org/10.1016/j.apradiso.2009.02.030
14. E. Koumarianou, D. Pawlak, A. Korsak et al., Comparison of receptor affinity of ^{nat}Sc-DOTA-TATE versus ^{nat}Ga-DOTA-TATE. Nucl. Med. Rev. **14**, 85 (2011). https://doi.org/10.5603/NMR.2011.00021
15. F. Roesch, Scandium-44: benefits of a long-lived PET radionuclide available from the (44)Ti/(44)Sc generator system. Curr. Radiopharm. **5**, 187 (2012). https://doi.org/10.2174/1874471011205030187
16. M. Al-Abyad, I. Spahn, S.M. Qaim, Experimental studies and nuclear model calculations on proton induced reactions on manganese up to 45 MeV with reference to production of ^{55}Fe, ^{54}Mn and ^{51}Cr. Appl. Rad. Isot. **68**, 2393 (2010). https://doi.org/10.1016/j.apradiso.2010.06.013
17. M. Sadeghi, M. Enferadib, H. Nadib, ^{45}Ti, a candidate for positron emission tomography: study of the cyclotron production. Radiochemistry **53**, 411 (2011). https://doi.org/10.1134/S106636221104014X
18. C.H.M. Broeders, A. Yu. Konobeyev, Yu. A. Korovin et al., FZK 7183, ALICE/ASH manual (2006). http://bibliothek.fzk.de/zb/berichte/FZKA7183.pdf. Accessed 19 June 2017
19. Experimental Nuclear Reaction Data (EXFOR), (2017). https://www-nds.iaea.org/exfor/exfor.htm. Accessed 19 June 2017
20. A.J. Koning, D. Rochman, J. Kopecky et al., TENDL-2015: TALYS-based evaluated nuclear data library. http://www.talys.eu/home/. Accessed 19 June 2017
21. M. Sadeghi, N. Soheibi, T. Kakavand et al., Targetry and nuclear data for the cyclotron production of ^{55}Fe via various reactions. J. Radioanal. Nucl. Chem. **293**, 1 (2012). https://doi.org/10.1007/s10967-012-1719-9
22. M. Sadeghi, M. Enferadi, Nuclear model calculations on the production of ^{119}Sb via various nuclear reactions. Ann. Nucl. Energy **38**, 825 (2011). https://doi.org/10.1016/j.anucene.2010.11.014
23. M. Sadeghi, N. Zandi, M. Bakhtiari, Nuclear model calculation for cyclotron production of ^{61}Cu as a PET imaging. J. Radioanal. Nucl. Chem. **292**, 777 (2012). https://doi.org/10.1007/s10967-011-1557-1
24. M. Sadeghi, M. Bakhtiari, M.K. Bakht et al., Overview of mercury radionuclides and nuclear model calculations of 195Hgm, g and 197Hgm, g to evaluate experimental cross section data. Phys. Rev. C **85**, 034605 (2012). https://doi.org/10.1103/PhysRevC.85.034605
25. M. Sadeghi, M. Enferadi, M. Aref et al., Nuclear data for the cyclotron production of ^{66}Ga, ^{86}Y, ^{76}Br, ^{64}Cu and ^{43}Sc in PET imaging. Nukleonika **55**, 293 (2010)
26. M. Yiğit, Investigating the (p, n) excitation functions on 104–106,108,110Pd isotopes. Appl. Rad. Isot. **130**, 109 (2017). https://doi.org/10.1016/j.apradiso.2017.09.027
27. M. Yiğit, A. Kara, Model-based predictions for nuclear excitation functions of neutron-induced reactions on $^{64,66-68}$Zn targets. Nucl. Eng. Technol. **49**, 996 (2017). https://doi.org/10.1016/j.net.2017.03.006
28. M.E. Korkmaz, M. Yiğit, O. Ağar, Excitation functions of neutron induced nuclear reactions for ^{59}Co nucleus using different level density models. Acta Phys. Pol. A **132**, 670 (2017). https://doi.org/10.12693/APhysPolA.132.670
29. M. Yiğit, E. Tel, Study on (n,2n) and (n, p) reactions of strontium nucleus. Nucl. Eng. Des. **293**, 97 (2015). https://doi.org/10.1016/j.nucengdes.2015.07.043
30. H. Korkut, T. Korkut, A. Kara et al., Monte carlo simulations of 17.9–22.3 MeV energetic proton irradiation effects on bcc-zirconium fusionic materials. J. Fusion Energ. **35**, 591–596 (2016). https://doi.org/10.1007/s10894-016-0068-z
31. M. Yiğit, E. Tel, Theoretical study of deuteron induced reactions on ^{6,7}Li, ^{9}Be and ^{19}F targets. Kerntechnik **79**, 63 (2014). https://doi.org/10.3139/124.110394
32. E. Tel, M. Yiğit, G. Tanır, Cross sections calculations of (d, t) nuclear reactions up to 50 MeV. J. Fusion Energy **32**, 273 (2013). https://doi.org/10.1007/s10894-012-9564-y
33. V.F. Weisskopf, D.H. Ewing, On the yield of nuclear reactions with heavy elements. Phys. Rev. **57**, 472 (1940). https://doi.org/10.1103/PhysRev.57.472
34. M. Blann, Hybrid model for pre-equilibrium decay in nuclear reactions. Phys. Rev. Lett. **27**, 337 (1971). https://doi.org/10.1103/PhysRevLett.27.337
35. M. Blann, H.K. Vonach, Global test of modified pre-compound decay models. Phys. Rev. C **28**, 1475 (1983). https://doi.org/10.1103/PhysRevC.28.1475
36. A.V. Ignatyuk, G.M. Smirenkin, A. Tishin, Phenomenological description of energy dependence of the level density parameter. Sov. J. Nucl. Phys. **21**, 255 (1975)
37. A.V. Ignatyuk, K.K. Istekov, G.N. Smirenkin, Role of collective effects in the systematics of nuclear level densities. Yadernaja Fizika **29**, 875 (1979)
38. S.K. Kataria, V.S. Ramamurthy, M. Blann et al., Shell-dependent level densities in nuclear reaction codes. Nucl. Instrum. Methods Phys. Res. A **288**, 585 (1990). https://doi.org/10.1016/0168-9002(90)90155-Y
39. V.N. Levkovskij, *Book:Levkovskij, Act Cs. by Protons and Alphas* (USSR, Moscow, 1991)
40. R. Ejnisman, I.D. Goldman, P.R. Pascholati et al., Cross sections for ^{45}Sc(p,2n)^{44}Ti and related reactions. Phys. Rev. C **54**, 2047 (1996). https://doi.org/10.1103/PhysRevC.54.2047
41. J.W. Meadows, R.M. Diamond, R.A. Sharp, Excitation functions and yield ratios for the isomeric pairs Br 80,80 m, Co58,58 m,

and Sc44,44 m formed in (p, pn) reactions. Phys. Rev. **102**, 190 (1956). https://doi.org/10.1103/PhysRev.102.190

42. T. Mcgee, C.L. Rao, G.B. Saha et al., Nuclear interactions of ^{45}Sc and ^{68}Zn with protons of medium energy. Nucl. Phys. A **150**, 11 (1970). https://doi.org/10.1016/0375-9474(70)90451-3
43. A.J. Howard, H.B. Jensen, M. Rios et al., Measurement and theoretical analysis of some reaction rates of interest in silicon burning. Astrophys. J. **188**, 131 (1974). https://doi.org/10.1086/152694
44. R.G. Thomas, W. Bartolini, Excitation functions for (p, n) and (p,2n) interactions in Sc, Cr, Mo, Cd and W between 8 and 14 MeV. Nucl. Phys. A **106**, 323 (1968). https://doi.org/10.1016/0375-9474(67)90877-9
45. F. Ditroi, F. Tarkanyi, S. Takacs et al., Activation cross sections of longer lived products of proton induced nuclear reactions on manganese up to 70 MeV. Nucl. Instrum. Methods Phys. Res. B **308**, 34 (2013). https://doi.org/10.1016/j.nimb.2013.04.058
46. R. Michel, G. Brinkmann, On the depth-dependent production of radionuclides ($44 \leq A \leq 59$) by solar protons in extraterrestrial matter. J. Radioanal. Nucl. Chem. **59**, 467 (1980). https://doi.org/10.1007/BF02517298
47. M. Gusakow, G. Albouy, N. Poffe et al., Reactions (p, pn) a moyenne energie. Journal de Physique **22**, 636 (1961). https://doi.org/10.1051/jphysrad:019610022010063600
48. R.C. Albert, (p, n) Cross section and proton optical-model parameters in the 4 to 5.5 MeV energy region. Phys. Rev. **115**, 925 (1959). https://doi.org/10.1103/PhysRev.115.925
49. C.H. Johnson, C.C. Trail, A. Galonsky, Thresholds for (p, n) reactions on 26 intermediate weight nuclei. Phys. Rev. **136**, B1719 (1964). https://doi.org/10.1103/PhysRev.136.B1719
50. G.F. Dell, W.D. Ploughe, H.J. Hausman, Total reaction cross sections in the mass range 45 to 65. Nucl. Phys. **64**, 513 (1965). https://doi.org/10.1016/0029-5582(65)90576-6